JOURNAL OF MATERIALS SCIENCE **38** (2003) 1809–1817

Multiple film cracking in film/substrate systems with residual stresses and unidirectional loading

C. H. HSUEH
Metals and Ceramics Division, Oak Ridge National Laboratory, Oak Ridge, Tennessee 37831
M. YANAKA
Toppan Technical Research Institute, Sugito-machi, Kitakatsushika-gun, Saitama 345-8508, Japan

Multiple film cracking in film/substrate systems is analyzed in the present study. Specifically, the experimental measurements of multiple cracking of SiO_x films of various thicknesses on polyethylene terephthalate substrates are analyzed. The system is subjected to both residual stresses and unidirectional tensile loading. Considering a three-dimensional geometry, an analytical model is developed to derive the stress distribution in the system, and the film-cracking problem is analyzed using both the strength and the energy criteria. Compared to the strength criterion, the energy criterion shows better agreement with the measurements of the crack density versus applied strain relation.

1. Introduction

Cracking of brittle films on substrates is a major reliability problem in microelectronic devices, protective coatings, and other thin film applications [1]. The as-fabricated film/substrate system is generally subjected to residual stresses, which result from both the film deposition process and the thermo-mechanical mismatch between the film and the substrate. These residual stresses combined with stresses applied to the system can lead to cracking of the brittle film. Recently, a transparent gas barrier layer consisting of a submicron thick SiO_x film deposited on a polyethylene terephthalate (PET) substrate was developed for food and medical packaging applications to replace the conventional aluminum metalized foil [2, 3]. The durability of the SiO_x/PET system relies critically on the integrity of the SiO_x film during the fabrication process and in service. To characterize the film strength, the technique of multiple film cracking has been used in which the film/substrate system is loaded unidirectionally [4–10]. As the system is stretched, cracks transverse to the loading direction develop in the film. The number of cracks increases as the applied strain is increased, and the relation between the measured crack density (i.e., the number of cracks per unit length) and the applied strain has been used to characterize the film strength.

To quantitatively analyze the film-cracking problem, the complete stress distribution in the system is required. Stress transfer occurs between the film and the substrate during the loading and cracking processes. The classical analytical model in analyzing the stress transfer problem is the shear lag model, which was originally developed by Cox [11] to analyze the stress transfer between the fiber and the matrix in a fiber-reinforced composite. Adopting the concept of the shear lag model with a cylindrical geometry, the stress transfer between the film and the substrate in a planar geometry has been analyzed [8, 12–15]; however, the analysis is limited to a two-dimensional geometry with the plane-strain or plane-stress approximation. When the system is subjected to both loading and residual stresses, this two-dimensional analysis is not applicable. The plane-strain approximation can be used when the system is subjected to only an applied load. On the other hand, the residual stresses in the system are bi-axial prior to cracking and become more complex after cracking. Also, it is noted that the stress transfer is dictated by the shear stress at the film/substrate interface. Depending upon the properties of the interface, two types of the shear lag model have been developed. The first one considers that the substrate is ductile and the interface yields such that the interfacial shear stress is governed by a constant yield strength of the substrate [12, 13]. In this case, the stress distribution in the system can be readily related to the yield strength. The second one considers the interface to be elastic and to remain bonded. In this case, the interfacial shear stress is often assumed to be proportional to the relative displacement between film and substrate, and a fitting parameter hence exists in the stress transfer solutions [8, 13, 14]. This fitting parameter can be determined by fitting theoretical results to experimental data.

Recently, an improved shear lag model has been developed to analyze the residual stresses in a film strip/substrate system in a three-dimensional sense [16], and the analytical results agree well with measurements; however, external loading was not included in the analysis. The purpose of the present study is to add the effects of external loading to this improved shear lag model [16] to analyze the stress distribution

in the system which is then incorporated with cracking criteria to analyze multiple film cracking in a three-dimensional sense. First, closed-form analytical solutions are derived to predict the stress distribution in a film segment when the film/substrate system is subjected to both residual stresses and loading, and both strength and energy criteria are then adopted to predict film cracking. Second, the previous experimental results of multiple film cracking [8] with some modifications are summarized. Finally, the predicted relation between the crack density and the applied strain is compared to the experimental measurements. Comparison is also made between the present analytical solution and an existing solution based on the energy release rate approach [17,18]. It is noted that the statistical effects on multiple film cracking have been analyzed elsewhere [19–22] and are not considered in the present analysis.

2. Analytical modeling

The film/substrate system is schematically shown in Fig. 1, in which the Cartesian coordinates, x, y, and z, are used. The film is bonded to the substrate at $x = 0$, and the free surfaces of the substrate and the film are located respectively at $x = -s$ and $x = t$, such that the thicknesses of the substrate and the film are respectively s and t. The film is subjected to a mismatch strain, $\Delta\varepsilon$, relative to the substrate before loading. A uniform strain, ε_a, is applied on the system in the y-direction. The film is cracked with a uniform crack spacing, $2l$, and a periodic array of film segments is formed. In this case, only one film segment is required in the analysis, and the y-coordinate is selected such that the ends of the selected film segment are located at $y = \pm l$. This film segment/substrate system (Fig. 1) has the same geometry as the film strip/substrate system in the previous study [16]. Compared to the boundary conditions in the previous study [16], the present boundary conditions have a free surface instead of a fixed surface at the substrate surface (i.e., at $x = -s$) plus the addition of an applied strain, ε_a, on the system.

When the system has an infinite length in the z-direction, there is no stress variation in the z-direction. The equilibrium equation between the normal stress, σ_y, and the shear stress, $\tau_{xy}(= \tau)$, is

$$\frac{\partial \sigma_y}{\partial y} + \frac{\partial \tau}{\partial x} = 0 \tag{1}$$

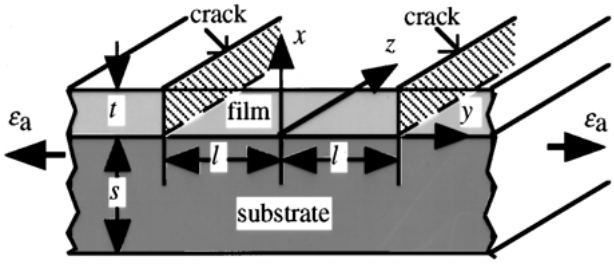

Figure 1 A schematic showing analytical modeling of multiple film cracking with a uniform crack spacing, $2l$, in a film/substrate system.

Integration of Equation 1 over the thickness of the film and then division by its thickness yield

$$\frac{\partial}{\partial y}\left(\frac{1}{t}\int_0^t \sigma_y dx\right) + \frac{1}{t}\int_0^t \frac{\partial \tau}{\partial x} dx = 0 \tag{2}$$

Because the film is relatively thin, the variation of σ_y through the thickness can be ignored. Letting σ_f represent the average value of σ_y over the thickness of the film and using the free surface condition that $\tau = 0$ at $x = t$, Equation 2 becomes

$$\frac{d\sigma_f}{dy} = \frac{\tau_0}{t} \tag{3}$$

where τ_0 is the shear stress at the interface (i.e., $\tau = \tau_0$ at $x = 0$). The stress gradient in the film is described by Equation 3.

To strictly satisfy the equilibrium equation, the stress-displacement relation, and the essential boundary conditions, solutions for the stress distribution require extensive numerical analysis. However, simple analytical solutions are attainable when some of the above equations are satisfied approximately and the rest of the equations are satisfied exactly. Because the main interest in the system is the variation of σ_y in the y-direction, an approximation of satisfying the equilibrium equation (Equation 1) in an average sense (with respect to the x-direction) is taken for the substrate. Hence, the gradient of σ_y in the y-direction in the substrate is approximated by a function of y in using Equation 1, such that

$$\frac{\partial \sigma_y}{\partial y} = f(y) \quad (\text{for } -s \le x \le 0) \tag{4}$$

It is noted that the same approximation has been adopted in analyzing the two-dimensional stress transfer problem for a plate embedded in a matrix, and the predicted stress distribution in the system agrees well with the finite element results [23]. The approximate x-dependence of σ_y can be obtained by solving the approximate equilibrium equation and is shown as follows.

Continuity of the shear stress at the interface (i.e., $\tau = \tau_0$ at $x = 0$) is required. Solution of Equations 1 and 4 subjected to the continuity condition and the free surface condition (i.e., $\tau = 0$ at $x = -s$) gives

$$\tau = \left(1 + \frac{x}{s}\right)\tau_0 \quad (\text{for } -s \le x \le 0) \tag{5}$$

With $\sigma_x = 0$ and the displacement in the x-direction being negligible, τ can be related to the displacement in the y-direction, w, by

$$\tau = \frac{E_s}{2(1+\nu_s)}\frac{dw}{dx} \quad (\text{for } -s \le x \le 0) \tag{6}$$

where E_s and ν_s are Young's modulus and Poisson's ratio of the substrate, respectively. Combination of Equations 5 and 6 and integration from $x = -s$ to

0 yield

$$\tau_0 = \frac{E_s\,(w_0 - w_s)}{s\,(1+\nu_s)} \tag{7a}$$

where w_0 and w_s are the displacements in the y-direction at $x = 0$ and $-s$, respectively. The shear stress, τ, can be obtained by substituting Equation 7a into Equation 5, such that

$$\tau = \left(1 + \frac{x}{s}\right)\frac{E_s(w_0 - w_s)}{s(1+\nu_s)} \quad (\text{for } -s \le x \le 0) \tag{7b}$$

The displacement, w, can be derived by combination of Equations 6 and 7b and integration from $x = -s$ to x, such that

$$w = w_s + \left(1 + \frac{x}{s}\right)^2 (w_0 - w_s) \quad (\text{for } -s \le x \le 0) \tag{8}$$

Differentiation of Equation 8 with respect to y and then multiplication by E_s give

$$\sigma_y = \sigma_s + \left(1 + \frac{x}{s}\right)^2 (\sigma_0 - \sigma_s) \quad (\text{for } -s \le x \le 0) \tag{9}$$

where $\sigma_y = \sigma_0$ at $x = 0$, and $\sigma_y = \sigma_s$ at $x = -s$. The approximate x-dependence of σ_y in the substrate is described by Equation 9. It is noted that the stresses, σ_y, σ_0, and σ_s, are functions of y and l which will be derived later.

The mechanical equilibrium condition between the applied strain ε_a and the stress distribution in the system is required. However, the resultant load due to the applied strain is required before formulating the equilibrium equation. The applied strain, ε_a, is imposed on the film/substrate system, the far-field stresses due to the applied strain are uniform in the film and the substrate respectively, and the compatibility condition requires

$$\frac{1}{E_f}\left(\sigma_y^f - \nu_f\sigma_z^f\right) = \frac{1}{E_s}\left(\sigma_y^s - \nu_s\sigma_z^s\right) = \varepsilon_a \tag{10a}$$

$$\frac{1}{E_f}\left(\sigma_z^f - \nu_f\sigma_y^f\right) = \frac{1}{E_s}\left(\sigma_z^s - \nu_s\sigma_y^s\right) \tag{10b}$$

where σ_y and σ_z are the far-field stresses in the y- and the z-directions, and the super/subscripts, f and s, denote the film and the substrate, respectively. Without constraints in the z-direction, the resultant load is zero in the z-direction. When the substrate is much thicker than the film, σ_z^s is zero in the substrate. With $\sigma_z^s = 0$ combination of Equations 10a and b yields

$$\sigma_y^s = E_s\varepsilon_a \tag{11a}$$

$$\sigma_y^f = \frac{(1-\nu_f\nu_s)E_f\varepsilon_a}{1-\nu_f^2} \tag{11b}$$

Hence, the mechanical equilibrium condition between the applied strain ε_a and the stress distribution in the film segment and the substrate is

$$\int_{-s}^{0}\sigma_y dx + t\sigma_f = \left[sE_s + \frac{t(1-\nu_f\nu_s)E_f}{1-\nu_f^2}\right]\varepsilon_a \tag{12}$$

Substitution of Equation 9 into Equation 12 gives

$$\sigma_s = -\frac{\sigma_0}{2} - \frac{3t\sigma_f}{2s} + \frac{3}{2}\left[E_s + \frac{t(1-\nu_f\nu_s)E_f}{s\left(1-\nu_f^2\right)}\right]\varepsilon_a \tag{13}$$

Differentiation of Equation 3 with respect to y and combination with Equations 7a and 13 yield

$$\frac{d^2\sigma_f}{dy^2} = \frac{3}{2st(1+\nu_s)}\left\{\sigma_0 + \frac{t}{s}\sigma_f - \left[E_s + \frac{t(1-\nu_f\nu_s)E_f}{s\left(1-\nu_f^2\right)}\right]\varepsilon_a\right\} \tag{14}$$

The solution of the stress distribution σ_f is contingent upon the determination of σ_0. For a bonded interface, the relation between σ_0 and σ_f can be derived from the displacement compatibility condition when the film is subjected to a mismatch strain, such that [16]

$$\sigma_0 = \frac{\left(1-\nu_f^2\right)E_s}{(1-\nu_f\nu_s)E_f}\sigma_f + \frac{(1+\nu_f)E_s}{1-\nu_f\nu_s}\Delta\varepsilon \tag{15}$$

Hence, the differential equation governing the stress distribution in the film can be obtained by substituting Equation 15 into Equation 14; i.e.,

$$\frac{d^2\sigma_f}{dy^2} = \frac{3}{2st(1+\nu_s)}\left\{\left[\frac{t}{s} + \frac{\left(1-\nu_f^2\right)E_s}{(1-\nu_f\nu_s)E_f}\right]\sigma_f + \frac{(1+\nu_f)E_s\Delta\varepsilon}{1-\nu_f\nu_s} - \left[E_s + \frac{t(1-\nu_f\nu_s)E_f}{s\left(1-\nu_f^2\right)}\right]\varepsilon_a\right\} \tag{16}$$

The solution of σ_f from Equation 16 subjected to the stress-free condition at $y = l$ and the symmetric condition at $y = 0$ is

$$\sigma_f = \frac{E_f}{1-\nu_f}\left[\frac{(1-\nu_f\nu_s)\varepsilon_a}{1+\nu_f} - \frac{\Delta\varepsilon}{1+\frac{t(1-\nu_f\nu_s)E_f}{s\left(1-\nu_f^2\right)E_s}}\right] \times\left[1 - \frac{\cosh(\alpha y)}{\cosh(\alpha l)}\right] \quad (\text{for } -l \le y \le l) \tag{17}$$

where

$$\alpha = \left[\frac{3}{2st(1+\nu_s)}\left(\frac{t}{s} + \frac{\left(1-\nu_f^2\right)E_s}{(1-\nu_f\nu_s)E_f}\right)\right]^{1/2} \tag{18}$$

The stress distribution along the film segment is described by Equation 17. The plane-strain nature [i.e., a factor of $E_f/(1-\nu_f^2)$] for the applied strain, ε_a, and the biaxial-stress nature [i.e., a factor of $E_f/(1-\nu_f)$]

for the mismatch strain, $\Delta\varepsilon$, can be readily seen in Equation 17.

2.1. Strength criterion for film cracking

The maximum stress within the film occurs at the middle of the film segment (i.e., at $y = 0$), such that

$$\sigma_{\mathrm{f}}^{\max} = \frac{E_{\mathrm{f}}}{1-\nu_{\mathrm{f}}}\left[\frac{(1-\nu_{\mathrm{f}}\nu_{\mathrm{s}})\varepsilon_{\mathrm{a}}}{1+\nu_{\mathrm{f}}} - \frac{\Delta\varepsilon}{1+\frac{t(1-\nu_{\mathrm{f}}\nu_{\mathrm{s}})E_{\mathrm{f}}}{s\left(1-\nu_{\mathrm{f}}^2\right)E_{\mathrm{s}}}}\right] \times [1-\operatorname{sech}(\alpha l)] \tag{19}$$

Cracking of the film segment will occur at $y = 0$ when $\sigma_{\mathrm{f}}^{\max}$ reaches the film strength, σ_{str}. The critical applied strain, ε_{c}, for film cracking to initiate can be obtained from Equation 19. When an uncracked film [i.e., $l \gg 0$ in Equation 19] is subjected to ε_{c}, the corresponding $\sigma_{\mathrm{f}}^{\max}$ reaches σ_{str}, such that

$$\sigma_{\mathrm{str}} = \frac{E_{\mathrm{f}}}{1-\nu_{\mathrm{f}}}\left[\frac{(1-\nu_{\mathrm{f}}\nu_{\mathrm{s}})\varepsilon_{\mathrm{c}}}{1+\nu_{\mathrm{f}}} - \frac{\Delta\varepsilon}{1+\frac{t(1-\nu_{\mathrm{f}}\nu_{\mathrm{s}})E_{\mathrm{f}}}{s\left(1-\nu_{\mathrm{f}}^2\right)E_{\mathrm{s}}}}\right] \tag{20}$$

The relation between the applied strain, ε_{a}, and the film segment with length $2l$ to break into two equal-length segments can be obtained from Equation 19 by substituting σ_{str} (Equation 20) in place of $\sigma_{\mathrm{f}}^{\max}$, such that

$$\varepsilon_{\mathrm{a}} = \frac{\cosh(\alpha l)\varepsilon_{\mathrm{c}} - \frac{1+\nu_{\mathrm{f}}}{1-\nu_{\mathrm{f}}\nu_{\mathrm{s}}}\frac{\Delta\varepsilon}{1+\frac{t(1-\nu_{\mathrm{f}}\nu_{\mathrm{s}})E_{\mathrm{f}}}{s\left(1-\nu_{\mathrm{f}}^2\right)E_{\mathrm{s}}}}}{\cosh(\alpha l)-1} \tag{21}$$

It is noted that the result of Equation 21 is based on the condition of a constant film strength during the film segmentation process.

2.2. Energy criterion for film cracking

For the problem considered in the present study, the following energy terms are involved: (1) the elastic strain energy in the film and the substrate, (2) the fracture energy of the film, and (3) the work done by external loading. For the geometry defined in Fig. 1, the stress in the film segment with length $2l$ is described by Equation 17 before film cracking occurs, and the stress in the z-direction, σ_{z}, can be derived from [16] such that

$$\sigma_{\mathrm{z}} = \frac{\nu_{\mathrm{f}}-\nu_{\mathrm{s}}}{1-\nu_{\mathrm{f}}\nu_{\mathrm{s}}}\left(\sigma_{\mathrm{f}} + \frac{E_{\mathrm{f}}\Delta\varepsilon}{1-\nu_{\mathrm{f}}}\right) - \frac{E_{\mathrm{f}}\Delta\varepsilon}{1-\nu_{\mathrm{f}}} \tag{22}$$

The elastic strain energy in the film segment, U_{f1}, per unit depth in the z-direction is

$$U_{\mathrm{f1}} = \frac{t}{2}\int_{-l}^{l}(\varepsilon_{\mathrm{f}}\sigma_{\mathrm{f}} + \varepsilon_{\mathrm{z}}\sigma_{\mathrm{z}})\,\mathrm{d}y \tag{23}$$

where the elastic strains in the y- and the z-directions, ε_{f} and ε_{z}, are related to the stresses, σ_{f} and σ_{z}, by

$$\varepsilon_{\mathrm{f}} = (\sigma_{\mathrm{f}} - \nu_{\mathrm{f}}\sigma_{\mathrm{z}})/E_{\mathrm{f}} \tag{24a}$$

$$\varepsilon_{\mathrm{z}} = (\sigma_{\mathrm{z}} - \nu_{\mathrm{f}}\sigma_{\mathrm{f}})/E_{\mathrm{f}} \tag{24b}$$

When cracking occurs at $y = 0$, two film segments of equal length, l, are formed. Redefining the coordinate position of $y = 0$ at the center of each film segment, the elastic strain energy in these two film segments, U_{f2}, is

$$U_{\mathrm{f2}} = t\int_{-l/2}^{l/2}(\varepsilon_{\mathrm{f}}\sigma_{\mathrm{f}} + \varepsilon_{\mathrm{z}}\sigma_{\mathrm{z}})\,\mathrm{d}y \tag{25}$$

where the stress distribution in each film segment, σ_{f}, can be obtained from Equation 17 by substituting l with $l/2$, and σ_{z} is related to σ_{f} by Equation 22. The elastic energy change in the film due to cracking, ΔU_{f}, is

$$\Delta U_{\mathrm{f}} = U_{\mathrm{f2}} - U_{\mathrm{f1}} \tag{26}$$

Compared to ΔU_{f}, the change in elastic strain energy in the substrate is negligible because the substrate is much thicker than the film, no cracking occurs in the substrate, and the system is subjected to a constant stain, ε_{a}. The energy required for film cracking, ΔG_{f}, is

$$\Delta G_{\mathrm{f}} = 2t\Gamma \tag{27}$$

where Γ is the film fracture energy. Also, since film cracking occurs at a fixed applied strain, ε_{a}, there is no change of work due to film cracking. Hence, the energy balance equation for film cracking becomes

$$\Delta U_{\mathrm{f}} + \Delta G_{\mathrm{f}} = 0 \tag{28}$$

Solution of Equations 22 to 28 yields

$$\Gamma = \frac{E_{\mathrm{f}}}{2\alpha(1-\nu_{\mathrm{f}})(1-\nu_{\mathrm{f}}\nu_{\mathrm{s}})^2} \times \left[\frac{(1-\nu_{\mathrm{f}}\nu_{\mathrm{s}})\varepsilon_{\mathrm{a}}}{1+\nu_{\mathrm{f}}} - \frac{\Delta\varepsilon}{1+\frac{t(1-\nu_{\mathrm{f}}\nu_{\mathrm{s}})E_{\mathrm{f}}}{s\left(1-\nu_{\mathrm{f}}^2\right)E_{\mathrm{s}}}}\right]^2 \times \left[P_1R_1 - \frac{P_2R_2\Delta\varepsilon}{\frac{(1-\nu_{\mathrm{f}}\nu_{\mathrm{s}})\varepsilon_{\mathrm{a}}}{1+\nu_{\mathrm{f}}} - \frac{\Delta\varepsilon}{1+\frac{t(1-\nu_{\mathrm{f}}\nu_{\mathrm{s}})E_{\mathrm{f}}}{s\left(1-\nu_{\mathrm{f}}^2\right)E_{\mathrm{s}}}}}\right] \tag{29}$$

where

$$P_1 = (1+\nu_{\mathrm{f}})\left(1-2\nu_{\mathrm{f}}\nu_{\mathrm{s}}+\nu_{\mathrm{s}}^2\right) \tag{30a}$$

$$P_2 = -2\nu_{\mathrm{s}}(1+\nu_{\mathrm{s}})\left(1-\nu_{\mathrm{f}}^2\right) \tag{30b}$$

$$R_1 = 4\tanh(\alpha l/2) - \frac{\exp(\alpha l)-\exp(-\alpha l)+2\alpha l}{\exp(\alpha l)+\exp(-\alpha l)+2} - 2\tanh(\alpha l) + \frac{1}{2}\frac{\exp(2\alpha l)-\exp(-2\alpha l)+4\alpha l}{\exp(2\alpha l)+\exp(-2\alpha l)+2} \tag{30c}$$

$$R_2 = 2\tanh(\alpha l/2) - \tanh(\alpha l) \tag{30d}$$

The critical applied strain, ε_{c}, for film cracking to initiate can be obtained from the solution of ε_{a} in

Equation 29 by letting $l \to \infty$, such that the relation between Γ and ε_c is

$$\Gamma = \frac{E_f}{2\alpha(1-\nu_f)(1-\nu_f\nu_s)^2} \times \left[\frac{(1-\nu_f\nu_s)\varepsilon_c}{1+\nu_f} - \frac{\Delta\varepsilon}{1+\frac{t(1-\nu_f\nu_s)E_f}{s(1-\nu_f^2)E_s}}\right]^2 \times \left[\frac{3P_1}{2} - \frac{P_2\Delta\varepsilon}{\frac{(1-\nu_f\nu_s)\varepsilon_c}{1+\nu_f} - \frac{\Delta\varepsilon}{1+\frac{t(1-\nu_f\nu_s)E_f}{s(1-\nu_f^2)E_s}}}\right] \quad (31)$$

Combination of Equations 29 and 31 yields

$$\varepsilon_a = \frac{-(1+\nu_f)\Delta\varepsilon}{(1-\nu_f\nu_s)}\left\{\frac{-1}{1+\frac{t(1-\nu_f\nu_s)E_f}{s(1-\nu_f^2)E_s}} + \frac{-P_2R_2+\sqrt{(P_2R_2)^2-4P_1R_1Q}}{2P_1R_1}\right\} \quad (32)$$

where

$$Q = \frac{-3P_1}{2}\left[\frac{1}{1+\frac{t(1-\nu_f\nu_s)E_f}{s(1-\nu_f^2)E_s}} - \frac{(1-\nu_f\nu_s)\varepsilon_c}{(1+\nu_f)\Delta\varepsilon}\right]^2 - P_2\left[\frac{1}{1+\frac{t(1-\nu_f\nu_s)E_f}{s(1-\nu_f^2)E_s}} - \frac{(1-\nu_f\nu_s)\varepsilon_c}{(1+\nu_f)\Delta\varepsilon}\right] \quad (33)$$

The relation between the applied strain, ε_a, and the film segment with length $2l$ to break into two equal-length segments is described by Equation 32, in which l is contained in R_1 and R_2.

3. Summary of experiments with modifications

Experiments of multiple film cracking have been performed on SiO_x/PET systems [8]. However, some data presented previously were not sufficiently accurate. For example, there were problems in the calibration required to accurately measure the elastic constants, and the biaxial-stress state of the film was not considered in calculating the residual stresses from the curvature of the system. These deficiencies have been corrected in the present study, and the experiments are summarized as follows.

Various thicknesses (43, 67, 90, 120, and 320 nm) of SiO_x films were deposited by vacuum evaporation on 12 μm thick PET substrates. The deposited films were uniform, amorphous and free of macroscale defects. The stress-strain curves of the bare substrate and the substrate with film were used to obtain Young's moduli of the substrate and the film/substrate system, respectively. These two Young's moduli were then used to derive Young's modulus of the film, E_f. The elastic constants of the system thus obtained were $E_f = 73$ GPa, $E_s = 4.84$ GPa, $\nu_s = 0.35$, $\nu_f = 0.17$, and the yield strain of the PET substrate was ~2.2%. It is noted that the measured film density is 2.35 ± 0.09 g/cm^3, which lies between the densities of bulk amorphous and crystallized SiO_2 glasses, 2.2 and 2.6 g/cm^3. As a result, Young's modulus of the film is about that of the bulk glass.

The film was subjected to residual compression upon cooling to the room temperature. The mismatch strain in the film relative to the substrate, $\Delta\varepsilon$, can be calculated from the measured radius of curvature and the elastic constants of the system. In a plane-stress case, the mismatch strain, $\Delta\varepsilon$, can be related to the radius of curvature, r, by [24]

$$\Delta\varepsilon = \frac{s^4E_s^2 + t^4E_f^2 + 2st(2s^2+2t^2+3st)E_sE_f}{6rst(s+t)E_sE_f} \quad (34)$$

When $s \gg t$, Equation 34 can be simplified, such that

$$\Delta\varepsilon = \frac{s^2(sE_s+4tE_f)}{6rt(s+t)E_f} \quad (\text{for } s \gg t) \quad (35)$$

In a biaxial-stress case, $\Delta\varepsilon$ can be obtained from Equation 34 or 35 by replacing E with $E/(1-\nu)$. Both the measured r and the calculated $\Delta\varepsilon$ based on Equation 34 with the biaxial-stress correction are listed in Table I.

A constant displacement rate was then applied unidirectionally to stretch the system. The critical applied strain, ε_c, to initiate film cracking for each film thickness was also listed in Table I, and the crack density was measured during the test. The micrographs of multiple cracking for a 43 nm thick SiO_x film on a PET substrate at three different applied strains, 1.91%, 2%, and 4%, are shown in Fig. 2. It is noted that the measured crack spacing had a statistical distribution around a mean value, $\bar{l}$. At a given applied strain, the longest segments would break into halves with more or less half lengths, while shorter segments would remain unbroken. Hence,

TABLE I The data of the measured radius of curvature, r, of the SiO_x/PET system, the calculated mismatch strain, $\Delta\varepsilon$, in the SiO_x film relative to the PET substrate, and of the measured critical applied strain, ε_c, for initial film cracking

SiO_x film thickness t (nm)	Radius of curvature r (mm)	Mismatch strain $\Delta\varepsilon$ (%)	Critical cracking strain ε_c (%)
43	9.38	0.59	1.91
67	7.62	0.50	1.49
90	5.58	0.55	1.38
120	7.1	0.35	1.05
320	4.69	0.30	0.68

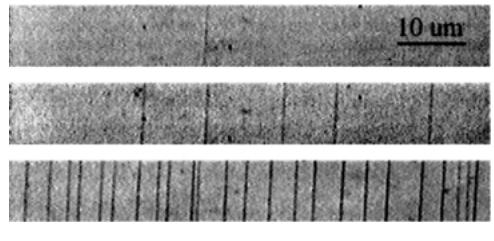

Figure 2 Micrographs of multiple cracking of 43 nm thick SiO_x film on a PET substrate at three different applied strains: upper 1.91% (crack onset strain), middle 2%, and lower 4%.

the longest and the shortest crack spacings would be $2l$ and l, respectively, when the applied strain is ε_a. The average crack spacing, $\bar{l}$, was approximated as the average of the longest and the shortest crack spacings, such that [8]

$$\bar{l} = \frac{3l}{2} \tag{36}$$

The measured crack density is the inverse of the average crack spacing; i.e., $1/\bar{l}$. It is also noted that the specimens were 100 mm in the y-direction (i.e., the loading direction) and 10 mm in the z-direction. Because the film is thin and brittle, the observed cracks always cut through the entire film thickness (i.e., the x-direction). While most of the cracks also cut through the z-direction, some cracks cut only partially through the z-direction; however, all cracks were more than 2 mm long in the z-direction. Because the film thickness ranges from 43 to 320 nm in the present study, it is appropriate to assume that the cracks are infinite long in the z-direction in the analysis.

4. Results

It has been argued that the thin film influences the stress field in the substrate only within a certain boundary zone in the neighborhood of the film. Outside the boundary zone, the stress field in the substrate is not perturbed by the presence of the film. Hence, an effective substrate thickness instead of the actual substrate thickness should be used in analytical modeling, and this effective substrate thickness is proportional to the film thickness [25]. Intuitively, the effective substrate thickness should also depend on the film width and the Young's modulus ratio of film to substrate. However, an analytical model for defining the effective substrate thickness has not been established. To find this effective substrate thickness, a finite element method is used in the present study. Half of the symmetric geometry is used in finite element modeling (see Fig. 3a), in which a thin film is bonded to a thick substrate, such that the half film width is 50 times of the film thickness and the substrate thickness is 145 times of the film thickness.

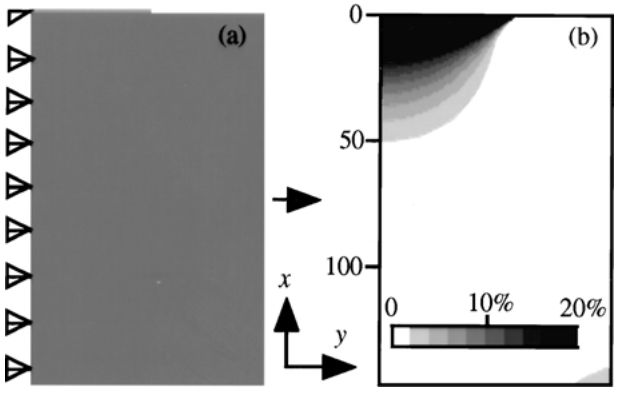

Figure 3 (a) A schematic showing the geometry used in FEA to determine the boundary zone, in which the stress field in the substrate is perturbed by the presence of the film, and (b) FEA results showing the perturbation of σ_y is less than 2% when the position in substrate is more than 50 times of the film thickness underneath the film.

While the right edge of the image in Fig. 3a is subjected to a uniform strain in the y-direction, the left edge is constrained from the movement in the y-direction to satisfy the symmetry condition. The elastic properties of the SiO_x/PET system are used and the plane strain condition is considered in the finite element analysis (FEA). The finite element result of the y-component stress in the substrate is shown in Fig. 3b, in which the perturbed stress is normalized by the far-field stress in the substrate (i.e., the one unperturbed by the presence of the film). It is shown in Fig. 3b that the perturbation is less than 2% when the position in the substrate is more than 50 times of the film thickness underneath the film. Hence, for the SiO_x/PET systems considered in the present study, the actual PET thickness (12 μm) is used in analytical modeling when SiO_x thickness is greater than 240 nm. However, for SiO_x thickness less than 240 nm, the effective substrate thickness is taken to be equal to 50 times of the film thickness.

4.1. Film strength and fracture energy

Using the data of the mismatch strain, $\Delta\varepsilon$, and the crack initiation strain, ε_c, in Table I as well as the elastic constants listed in Section 3, the strength and the fracture energy for initial film cracking can be calculated from Equations 20 and 31, respectively, and the results are shown in Fig. 4. Both the film strength, σ_{str}, and the fracture energy, Γ, show the trend of decreasement as the film thickness increases. However, while σ_{str} is approximately proportional to the inverse of the square root of the film thickness, Γ is relatively constant ($\sim$12 J/m^2) when the film thickness is less than 150 nm and decreases to $\sim$8 J/m^2 as the film thickness increases to 320 nm. The reported strain energy release rates for cracking of bulk amorphous and crystallized glasses are $\sim$8 and 20 J/m^2 [26], respectively, and the corresponding fracture energies are, $\sim$4 and 10 J/m^2, respectively. Hence, the calculated film fracture energy from the crack initiation strain is in the order of that for the bulk glass. The strain energy release rates of SiO_x films have previously been analyzed elsewhere using a two-dimensional shear lag model which are listed in the following for comparison. Ignoring the residual stresses in the shear lag model, Leterrier *et al*. obtained the strain energy release rate of $\sim$63 J/m^2 from measurements of multiple film cracking for film thicknesses ranging

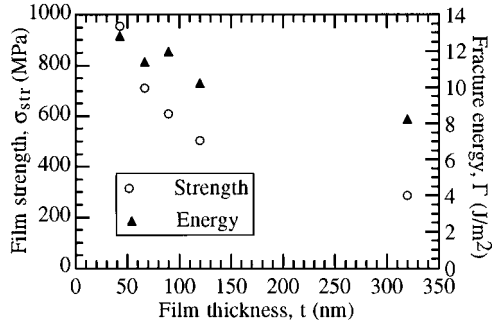

Figure 4 The calculated film strength, σ_{str}, and fracture energy, Γ, for the SiO_x film/PET substrate system based on the measured critical applied strain in initiating film cracking.

from 30 to 150 nm [7]. Assuming a shear deformation in the substrate in the shear lag model, the strain energy release rate obtained from the critical strain for initiating film cracking decreases from 70 to 23 J/m^2 when the film thickness increases from 43 to 320 nm [8]. However, when a shear deformation in the film is assumed in the shear lag model, the strain energy release rate becomes $\sim$1 J/m^2 [8].

4.2. Stress distribution in film segment

Two data sets, a low crack density (9.4 mm^{-1}) and a high crack density (187.5 mm^{-1}), of the 120 nm thick film from measurements are adopted in the present study to predict the stress distribution in the film segment to elucidate the essential trends. The critical applied strain for initial film cracking, ε_c, is 1.05%, and the corresponding crack density is 9.4 mm^{-1} (i.e., $l = 71\ \mu$m). When ε_a is increased to 2%, the corresponding crack density is 187.5 mm^{-1} (i.e., $l = 3.6\ \mu$m). Using Equation 17 and $\Delta\varepsilon = 0.35\%$ (Table I), the predicted stress distributions in the film segment are shown in Fig. 5a and b, respectively, for $l = 71\ \mu$m and 3.6 μm at different applied strains. The stress distribution in the film segment, $-l \leq y \leq l$, is symmetric with respect to the middle of the film (i.e., $y = 0$), and the stress distribution in half of the film segment, $0 \leq y \leq l$, is shown in Fig. 5.

The stress is zero at the end of the film segment (i.e., at the crack), and its magnitude increases with the distance from the crack and reaches an asymptotic value when the film segment is sufficiently long [e.g., see Fig. 5a]. In the absence of the applied strain, the residual stress in the film is compressive. The stress in the film, σ_f, becomes tensile when the applied tensile strain is sufficiently large. Film cracking is more likely to occur at positions with the highest tensile stress. For a long film segment [Fig. 5a], the region having the plateau value of σ_f extends from the middle of the film segment to a great distance which, in turn, results in a great area of potential locations for film cracking. Conversely, for a short film segment [Fig. 5b], the region with highest σ_f concentrates at the middle of the film segment and the potential locations for film cracking are limited to the middle area of the film. Hence, when film segmentation initially occurs, the lengths of the film segments have a great variation. The lengths of the film segments become more uniform in the later stage of film segmentation. This phenomenon is in agreement with the experimental observation [27].

4.3. Crack density

Using Equations 21 and 32, the predicted crack density, $1/\bar{l}$, versus the applied strain, ε_a, based on the strength and the energy criteria are shown in Fig. 6a, b, c, d, and e, respectively, for 43, 67, 90, 120, and 320 nm thick films. The experimental measurements are also shown. It is noted that limitations exist in the present analyses which are discussed as follows.

First, linear elasticity is considered in present analytical modeling. While the yield strain of the PET substrate is $\sim$2.2% [8], it was reported by Leterrier *et al.* that the permanent strain of the SiO_x/PET system upon unloading is negligible for an applied strain up to 4% [27]. In the presence of substrate plasticity, the load on the system is lower than that described by Equation 11 for a fixed applied strain ε_a, and the film should be subjected to a stress lower than that described by Equation 17 which, in turn, results in a smaller crack density than that predicted in Fig. 6. The effects of plasticity of the PET substrate were studied recently using a two-dimensional FEA [28]. The maximum stress in a film segment (which occurs at the middle of the film segment) obtained from elasto-plastic solutions is $\sim$5% lower than that obtained from elastic solutions when the applied strained is 4% [28]. When the applied strained is increased to 6%, the difference in the maximum film stress is increased to $\sim$7%. While plasticity's effects on the crack density versus applied strain relation are expected to be small, its effects on the crack density versus applied stress relation would become much greater.

Second, a constant strength or fracture energy of the film is considered in relating ε_a to $1/\bar{l}$ in the present analysis. The film strength, σ_{str}, or fracture energy, Γ, is derived from the critical strain, ε_c, in initiating film cracking. When a Weibull distribution of σ_{str} (or Γ) is considered, cracking should start from a lower value of σ_{str}, and σ_{str} increases progressively during the multiple cracking process. In this case, the predicted $1/\bar{l}$ at a fixed ε_a should be smaller than that based on a constant σ_{str} approach. However, since the film is uniform and

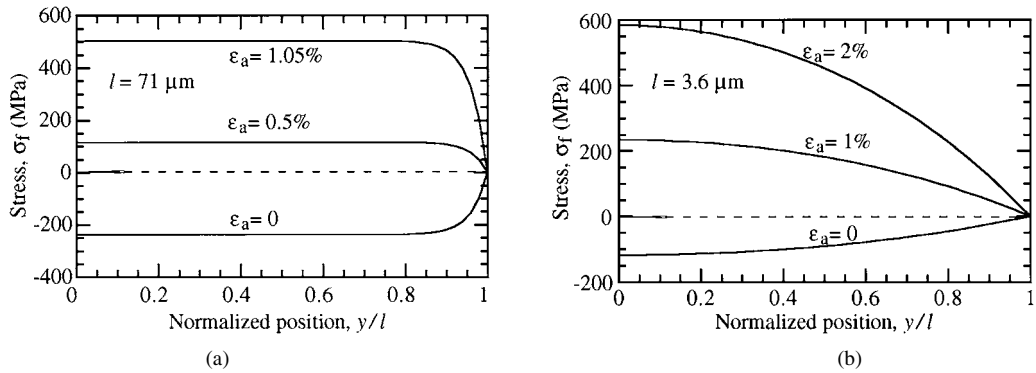

Figure 5 The predicted stress distribution, σ_f, along (a) a long film segment with half length $l = 71\ \mu$m, and (b) a short film segment with half length $l = 3.6\ \mu$m at different applied strains, ε_a, for a 120 nm thick SiO_x film on a PET substrate.

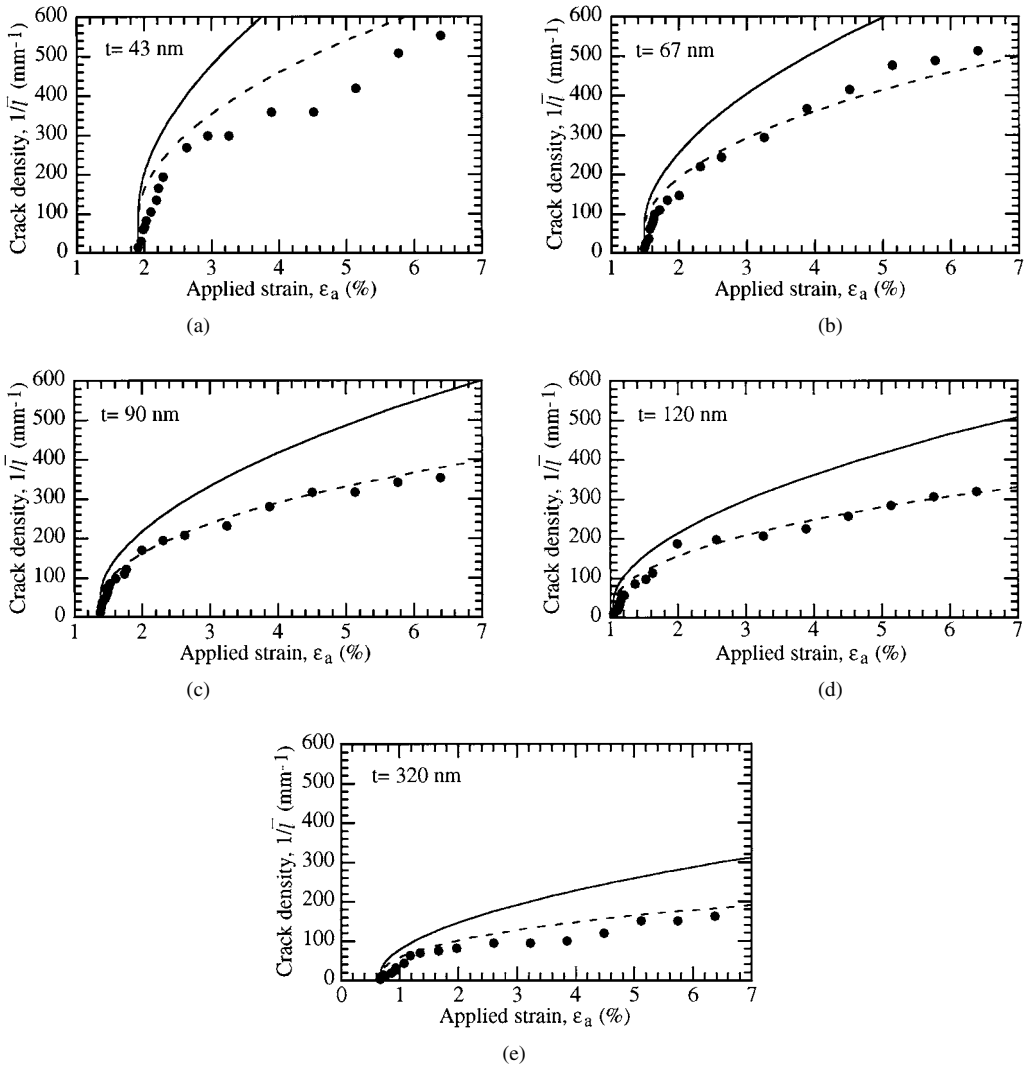

Figure 6 The predicted and the measured crack density, $1/\bar{l}$, as functions of the applied strain, ε_a, for film thicknesses, t, of (a) 43 nm, (b) 67 nm, (c) 90 nm, (d) 120, and (e) 320 nm in SiO_x/PET systems (——: strength criterion; - - - -: energy criterion; •: measurements).

free of macroscale defects, the Weibull distribution of σ_{str} is expected to be narrow.

Despite the limitations of the present analysis discussed above, good agreement is obtained for the crack density versus applied strain relation between the energy criterion-prediction and the measurement [Fig. 6a to e]. Compared to the energy criterion, the strength criterion predicts a greater crack density for fixed film thickness and applied strain.

4.4. Comparison with existing solution

Considering a periodic set of parallel edge cracks subjected to an opening stress in a semi-infinite plane, the energy release rate for cracks propagating perpendicular to the free surface has been analyzed by Tada *et al.* [17]. The solution was in a graphic form which was then fitted by a polynomial [17]. Based on Tada *et al.*'s solution, the change in strain energy to create a set of cracks of depth equal to the film thickness, t, has been derived by Thouless *et al.* [18]. Then, by minimizing the total energy of the cracked film (i.e., the strain energy in the cracked film and the fracture energy of the film), the relation between the equilibrium crack spacing, l, and the applied strain, ε, has been obtained, such that [18]

$$\frac{l}{t} \approx 5.6\sqrt{\frac{(1-\nu^2)\Gamma}{E\varepsilon^2 t}} \quad (\text{for } E\varepsilon^2 t/(1-\nu^2)\Gamma \geq 0.5) \tag{37}$$

It is noted that the above approximation is limited to the case that the film and the substrate have the same elastic properties.

The prediction of Equation 29 in the present study is compared to the above prediction [Equation 37]. To achieve this, the mismatch strain, $\Delta\varepsilon$, is ignored, the film and the substrate are assumed to have the same elastic properties, and $\nu = 0.25$ in using Equation 29. However, the effective substrate thickness [25] is required in order to complete the calculation. When the film and the substrate have the similar elastic constants, it has been shown by finite element analysis that the perturbation of the stress field in the substrate is negligible when the position in the substrate is 25 times of the film thickness away from the interface [29]. Assuming the effective substrate thickness be 10, 25, or 50 times of the film thickness, the predictions from Equation 29 are shown in Fig. 7 to compare with the prediction from

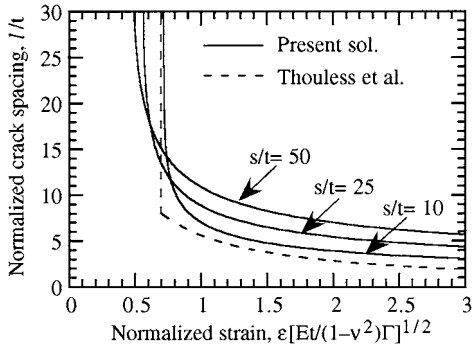

Figure 7 The normalized crack spacing, l/t, as a function of normalized strain, $\varepsilon[Et/(1-\nu^2)\Gamma]^{1/2}$ showing the comparison between the present prediction and Thouless *et al.*'s prediction.

Equation 37. While Equation 37 is an approximate solution, both Equations 29 and 37 show similar predictions in Fig. 7.

5. Conclusions

Experiments of multiple cracking of SiO_x films of various thicknesses on polyethylene terephthalate substrates (PET) were performed previously to characterize the film strength [8]. The system is subjected to both residual stresses and unidirectional tensile loading. Existing models to analyze the multiple film cracking problem are often limited to two-dimensional analyses. However, it is noted that while the applied stress can be analyzed using the plane-strain approximation, the residual stress in the film/substrate system is in a biaxial-stress state prior to cracking and becomes more complex after cracking. Considering a three-dimensional geometry, an analytical model is developed in the present study to derive the stress distribution in the system, and the film-cracking problem is analyzed using both the strength and the energy criteria. The analytical solution for the stress distribution in the film (Equation 17) contains the plane-strain nature for the applied stress and the biaxial-stress nature for the residual stress. Compared to the strength criterion, the energy criterion shows a better agreement with the measurements in the crack density versus applied strain relation. Compared to other analytical models, the present analytical model predicts a more reasonable fracture energy for the SiO_x film (which is in the order of the fracture energy of bulk glass) based on measurements of the critical strain in initiating film cracking. Also, fair agreement is obtained in comparing the present prediction (Equation 29) with the prediction of Equation 37, which is an approximate solution for the case that the film and the substrate have the same elastic properties.

Acknowledgements

The authors thank Dr. P. F. Becher, Prof. G. M. Pharr, and Dr. M. J. Lance for reviewing the manuscript. Research jointly sponsored by U.S. Department of Energy, Division of Materials Sciences and Engineering, Office of Basic Energy Sciences, under contract DE-AC05-00OR22725 with UT-Battelle (CHH), and Mr. Wada, Director of the Material Analysis Research Laboratory of Toppan Technical Research Institute (MY).

References

1. W. D. NIX, *Metall. Trans.* **20A** (1989) 2217.
2. J. RICE, *Food Process* June (1992) 78.
3. J. T. FELTS, *J. Plas. Film Sheet* **9** (1993) 139.
4. J. C. GROSSKREUTZ and M. B. MCNEIL, *J. Appl. Phys.* **40** (1969) 355.
5. F. FAUPEL, C. H. YANG, S. T. CHEN and P. S. HO, *ibid.* **65** (1989) 1911.
6. T. R. WATKINS and D. J. GREEN, *J. Amer. Ceram. Soc.* **76** (1993) 3066.
7. Y. LETERRIER, J. ANDERSONS, Y. PITTON and J.-A. E. MÅNSON, *J. Polym. Sci. B: Polym. Phys.* **35** (1997) 1463.
8. M. YANAKA, T. MIYAMOTO, Y. TSUKAHARA and N. TAKEDA, *Composite Interfaces* **6** (1999) 409.
9. H. BORDET, M. IGNAT and M. DUPEUX, *Thin Solid Films* **315** (1998) 207.
10. B. F. CHEN, J. HWANG, G. P. YU and J. H. HUANG, *ibid.* **352** (1999) 173.
11. H. L. COX, Brit. *J. Appl. Phys.* **3** (1952) 72.
12. M. S. HU and A. G. EVANS, *Acta Metall.* **37** (1989) 917.
13. F. S. SHIEU, R. RAJ and S. L. SASS, *Acta Metall. Mater.* **38** (1990) 2215.
14. N. LAWS and G. J. DVORAK, *J. Compos. Mater.* **22** (1988) 901.
15. C. H. HSUEH, *J. Amer. Ceram. Soc.* **84** (2001) 2955.
16. *Idem.*, *J. Appl. Phys.* **88** (2000) 3022.
17. H. TADA, P. C. PARIS and G. R. IRWIN, "The Stress Analysis of Cracks Handbook" (Paris Production, Inc., St. Louis, Missouri, 1985) p. 15.1.
18. M. D. THOULESS, E. OLSSON and A. GUPTA, *Acta Metall. Mater.* **40** (1992) 1287.
19. P. R. RAMSEY, H. W. CHANDLER and T. F. PAGE, *Thin Solid Films* **201** (1991) 81.
20. E. DELANNAY and P. WARREN, *Acta Metall. Mater.* **39** (1991) 1061.
21. J. H. SELVERIAN and D. O'NEIL, *Thin Solid Films* **235** (1993) 120.
22. A. MÉZIN and B. Sajid, *ibid.* **358** (2000) 46.
23. C. H. HSUEH, E. R. FULLER, S. A. LANGER and W. C. CARTER, *Mater. Sci. Eng.* A **268** (1999) 1.
24. C. H. HSUEH and A. G. EVANS, *J. Amer. Ceram. Soc.* **68** (1985) 241.
25. G. P. CHEREPANOV, *J. Appl. Phys.* **75** (1994) 844.
26. B. LAWN and R. WILSHAW, "Fracture" (Cambridge University Press, 1975) p. 77.
27. Y. LETERRIER, L. BOOGH, J. ANDERSONS and J.-A. E. MÅNSON, *J. Polym. Sci. B: Polym. Phys.* **35** (1997) 1449.
28. M. YANAKA, Y. TSUKAHARA, T. OKABE and N. TAKEDA, *J. Appl. Phys.* **90** (2001) 713.
29. S. C. JAIN, A. H. HARKER, A. ATKINSON and K. PINARDI, *ibid.* **78** (1995) 1630.

Received 17 October 2001
and accepted 8 January 2003